WARSAW UNIVERSITY OF TECHNOLOGY Index 351733
FACULTY OF CIVIL ENGINEERING
COMMITTEE FOR CIVIL AND WATER ENGINEERING
POLISH ACADEMY OF SCIENCES ISSN 1230-2945

DOI: 10.24425/ace.2026.157475

ARCHIVES OF CIVIL ENGINEERING

Vol. LXXII ISSUE 1 2026

pp. 301 –316

Research paper

Uniaxial compression experiments and numerical simulations of artificial rock samples with regular dentate discontinuity

Liangxiao Xiong[1], Suming Hu[2], Maolin Xue[3], Zhongyuan Xu[4]

Abstract: To study the uniaxial compression performance of rock masses with regular dentate discontinuities, uniaxial compression tests and Particle Flow Code (PFC) numerical simulation are conducted on cement mortar specimens, and the combined effects of dip angle γ, undulation angle β, and the number of undulating structures n of cracks on the compressive strength and crack propagation in the specimens are studied. The experimental and numerical simulation results showed that when n and β remain unchanged, the uniaxial compressive strength of the specimens peaks at a γ of 90°. When γ and β remain unchanged, the compressive strength of the specimens with regular dentate discontinuities decreases with an increase in n. When n and γ remain unchanged, the compressive strength of the rock mass specimens containing dentate discontinuity decreases with an increase in β. Almost all of the new cracks in the specimens initiate at the tip of the prefabricated cracks, and the failure characteristics of the specimens are mainly tensile fractures accompanied by a few shear fractures. When β and n remain unchanged, and γ is 45°–135°, the cracks in the dentate discontinuous rock mass propagate straight along the end of the prefabricated crack and finally vertically. In addition, when γ and n remain unchanged, the crack propagation of rock mass with $\beta \leq 60°$ is abundant. Moreover, when γ and β remain unchanged and $n < 4$, the crack propagation is abundant, and shear cracks are initiated at the edge of the specimens far from the prefabricated crack.

Keywords: uniaxial compression, dentate discontinuity, undulating angles, parallel bonded model

[1]Associate Prof., PhD., Eng., School of Civil Engineering and Architecture, East China Jiaotong University, Nanchang 330013, China, e-mail: xionglx1982@126.com, ORCID: 0000-0002-6366-5187

[2]Eng., School of Civil Engineering and Architecture, East China Jiaotong University, Nanchang 330013, China, e-mail: hsmcka@126.com, ORCID: 0009-0002-5752-043X

[3]Eng., China Construction Eighth Engineering Division Corp. Ltd., Southwest Branch, Chengdu 610059, China, e-mail: 18683342595@163.com, ORCID: 0000-0001-7725-690X

[4]PhD, Faculty of Geosciences and Environmental Engineering, Southwest Jiaotong University, Chengdu 611756, China, e-mail: zyxu@swjtu.edu.cn, ORCID: 0000-0003-4303-1870

1. Introduction

The numerous intricate joints and cracks present in natural rock reduce the mechanical properties of the rock mass, which creates challenges in geotechnical engineering practices.

Scholars worldwide have conducted extensive research on crack initiation, propagation, and coalescence in fractured rock mass under compression. In particular, related studies based on indoor modeling began at the end of the last century. Brace *et al*. [1] conducted compression experiments on a single prefabricated rock mass specimen containing inclined fractures. They found that an increase in loading under no or low confining pressure caused micro-cracks to appear at the tip of the prefabricated fracture that gradually bent toward the loading direction along the prefabricated crack and finally approached the principal stress direction. Some scholars also verified the law of wing crack initiation and propagation through theory and experiments and proposed a wing crack model based on their results (Horii *et al*. [2,3]; Ashby *et al*. [4]). Bobet *et al*. [5] conducted uniaxial and biaxial compression tests to study crack propagation using prefabricated rock mass specimens containing dentate discontinuity. Wong *et al*. [6] conducted a uniaxial compression test in sandstone materials containing two prefabricated cracks under different crack dip and bridge angles to obtain the strength law of dentate discontinuity in prefabricated rock mass specimens and the merge mode of three types of the main cracks. Lee *et al*. [7] studied the crack initiation, propagation, and coalescence of three materials containing prefabricated cracks under uniaxial compression and used the two-dimensional Particle Flow Code (PFC2D) program to develop a numerical simulation model shown to be in good agreement with the experimental results. Zhang *et al*. [8] conducted a series of uniaxial compression tests on pre-cracked rock specimens to investigate the influence of flaw geometry on the deformation and failure mechanisms of rock masses, with particular emphasis on evolutionary behavior of crack propagation under compressive loading. Qi *et al*. [9] conducted experimental compression tests on rock specimens containing three distinct types of pre-existing flaws, complemented by numerical simulations using PFC2D. It provided a systematic framework into the evolutionary mechanisms of crack propagation under compressive loading.

Dentate cracks are common types of fissures that are widely developed in natural slopes of hard rock masses and excavation engineering slopes. Many scholars have conducted experiments and numerical simulations based on the shear mechanical properties of rock masses containing dentate cracks. As early as 1994, Kodikara & Johnston [10] studied the shear mechanical properties of regular and irregular dentate discontinuities in rock–concrete joints under constant normal stress and constant normal stiffness and found that the brittle damage of regular jagged joints under normal stiffness is stronger than that of irregular jagged joints. Haberfield & Johnson [11] detailed the failure mechanism of rock mass specimens with dentate discontinuity during the shearing process and found that joint roughness plays a major role in the shear behavior of rock joints. Homand *et al*. [12] conducted a cyclic direct shear test on granite with prefabricated dentate discontinuity by analyzing the morphological evolution of the dentate discontinuity area of before and after shearing to quantitatively determine that the damaged area of the discontinuity increased with an increase in normal stress under low normal stress cyclic shear. Kwon *et al*. [13] used plaster materials with rectangular discontinuity specimens of different undulation heights to conduct shear tests to obtain the relationship between the shear

strength of the rough structure of the unit and the shear displacement. Bahaaddini *et al*. [14,15] used PFC2D to study the shear behavior of rock with dentate discontinuity and analyzed the influence of joint length on the peak shear behavior of the rock mass. The final numerical simulation and physical experiment were in good agreement with consistent shear intensity. Yin *et al*. [16] performed conventional triaxial compression and pre-peak unloading tests on saw-toothed fracture specimens under varying initial confining pressures. Their experimental results revealed the unloading-induced shear sliding response of rough fracture surfaces and the corresponding variations in interfacial shear strength. Li *et al*. [17] employed 3D printing technology to fabricate a series of specimens with irregular saw-toothed structures, which were subsequently subjected to direct shear tests and parallelized PFC simulations. Their study systematically investigated the evolution of micro-cracks and the distribution characteristics of force chains associated with rock discontinuities during the shearing process.

Although the literature includes abundant compression tests and numerical simulation studies on crack propagation in fractured rock masses as well as direct shear tests and numerical simulation on rock masses with dentate discontinuity, few researchers have conducted uniaxial compression tests on rock masses with dentate discontinuity. In this study, indoor uniaxial compression tests and PFC numerical simulations are conducted on mortar specimens with regular dentate discontinuities. The influence of the dip angle γ, undulation angle β, and the number of undulating structures n on the compressive strength and crack propagation in the rock mass is evaluated.

2. Experimental design

2.1. Specimen preparation

This study experimentally investigates rock mass specimens with undulated structural planes through a series of uniaxial compression tests. The specimens were composed of cement mortar with a water-to-cement ratio of 0.65 containing 325-type cement and ISO standard sand with particle sizes of 0.5–1.0 mm. Three intact specimens were subjected to uniaxial compression tests at a 1 mm/min loading rate to obtain their physical and mechanical parameters, which provides the basis for determining normal stress in the uniaxial compression test. The average values of physical and mechanical parameters of the experimental results of three intact specimens are shown in Table 1.

Table 1. Physical and mechanical parameters of intact rock-like specimens under uniaxial compression

Material	**Uniaxial compressive strength σ (MPa)**	**Elastic Modulus E (GPa)**	**Density ρ (g·cm^{-3})**
Rock-like cement mortar	25.14	1.73	2.05

The dimensions of the specimens used in this study were 100 mm × 100 mm × 100 mm. The mortar was poured into the mold, and after sufficient vibration, the required plastic plates of various widths and 1 mm thickness were inserted into the bottom of the mold. Then, the plastic

plates were removed before the initial mortar was set, and the specimens were cured at room temperature for 24 h before demolding. After the production was completed, the specimens were placed in water for 28 days to cure before being dried for testing. Figure 1 presents schematic diagrams of uniaxial compression for the specimens with regular dentate discontinuities.

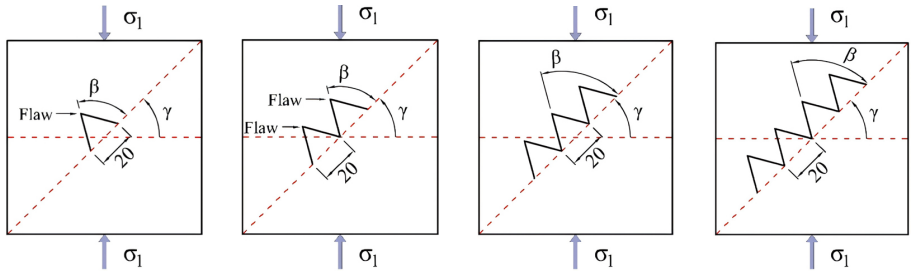

Fig. 1. Schematic diagram of uniaxial compression for specimens with regular dentate discontinuity: (a) $n = 1$; (b) $n = 2$; (c) $n = 3$; (d) $n = 4$

In the figures, dip angle γ is the angle between the bottom line of the undulating shape and the horizontal line, undulating angle β is the angle between the bottom line of the undulating structure and the left line of the undulating shape, and the number of undulating structures n is the number of undulating structures in the dentate discontinuity. Among them, the two sides of each undulating structure in the rock mass with regular dentate discontinuity were equal, and the vertex angle of the undulating structure with a regular dentate discontinuity was a right angle. The length of the bottom edge of each undulating structure in the rock mass with both regular dentate discontinuities was 20 mm. Figure 1 shows that n is 1, 2, 3, and 4, respectively, when γ and β are unchanged.

This test was conducted to determine the influence of the combination of γ, β, and n on the compressive strength and crack propagation of the specimens.

2.2. Test grouping

In this test, according to the combined changes of n, β, and γ, the compression tests of the specimens with regular dentate discontinuities were grouped, with 144 cases in total, as shown in Table 2, respectively.

Table 2. Test grouping of specimens with regular dentate discontinuity

n	β (°)	γ (°)
1	30, 45, 60, 75	0, 30, 45, 60, 90, 120, 135, 150, and 180
2	30, 45, 60, 75	0, 30, 45, 60, 90, 120, 135, 150, and 180
3	30, 45, 60, 75	0, 30, 45, 60, 90, 120, 135, 150, and 180
4	30, 45, 60, 75	0, 30, 45, 60, 90, 120, 135, 150, and 180

2.3. Experiment procedure

This experiment was conducted using a CSS-44300 microcomputer-controlled electronic universal testing machine, the experimental test system is shown in Fig. 2. During the experiment, the computer screen directly displayed the curves and the measured values of the test force, deformation, and displacement. The maximum axial pressure was 300 kN. The loading method of this test adopted displacement loading at a rate of 1 mm/min. For each case in the test group, three identical specimens were created.

Fig. 2. Mechanical property testing system

3. Test results

3.1. Influence of γ on the compressive strength of the specimens

Figure 3 shows the influence of various γ on the uniaxial compressive strength of the rock mass specimens with dentate discontinuity when n and β remained unchanged. The compressive strength assumed the peak point of the stress–strain curves.

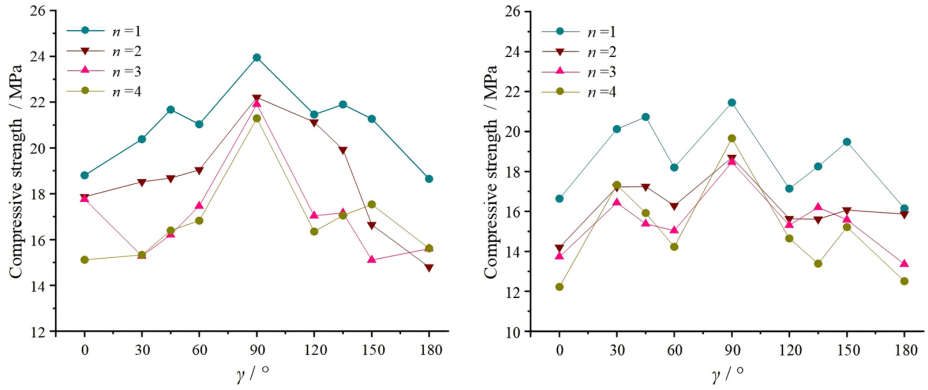

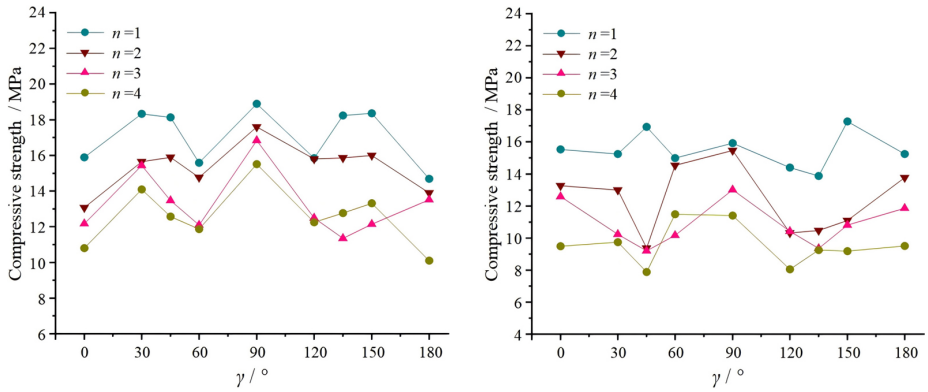

Fig. 3. Influence of various γ on the uniaxial compressive strength of the specimens for each selected n and β: (a) $\beta = 30°$; (b) $\beta = 45°$; (c) $\beta = 60°$; (d) $\beta = 75°$

Figure 3 presents the experimental results of rock mass compressive strength as a function of orientation angle γ, with parameters n and β held constant. The compressive strength reaches its minimum at $\gamma = 0°$ and 180°, and exhibits a trend of initial increase followed by a decrease as γ increases, reaching a peak at $\gamma = 90°$. In accordance with the Mohr-Coulomb criterion, when the inclination angle of the specimen exceeds the internal friction angle, the shear force along the structural plane surpasses the frictional resistance, resulting in reduced strength. Conversely, when the frictional resistance exceeds the shear force, the strength is enhanced. At $\gamma = 60°$ and 120°, significant sliding occurs due to the undulated structural plane, leading to a notable decline in compressive strength. Whereas at $\gamma = 90°$, the end friction effect effectively restrains sliding along the joint plane, thereby maximizing the compressive strength.

3.2. Influence of β on the compressive strength of the specimens

Figure 4 shows the influence of various β on the uniaxial compressive strength of the rock mass specimens with dentate discontinuity when n and γ remained unchanged.

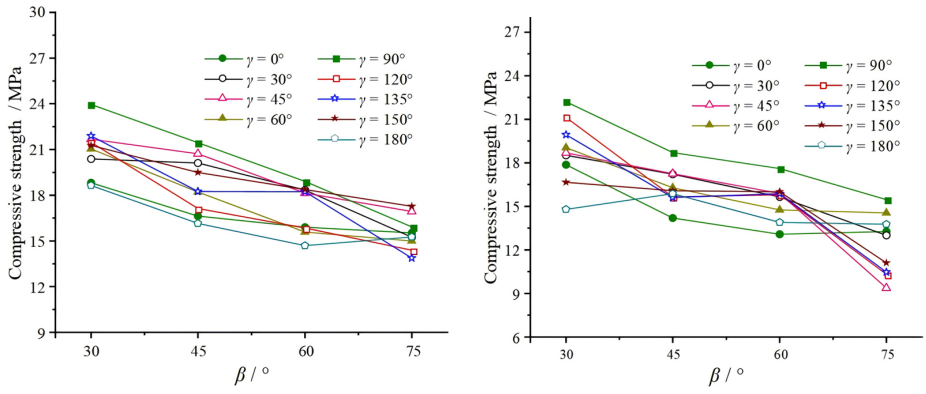

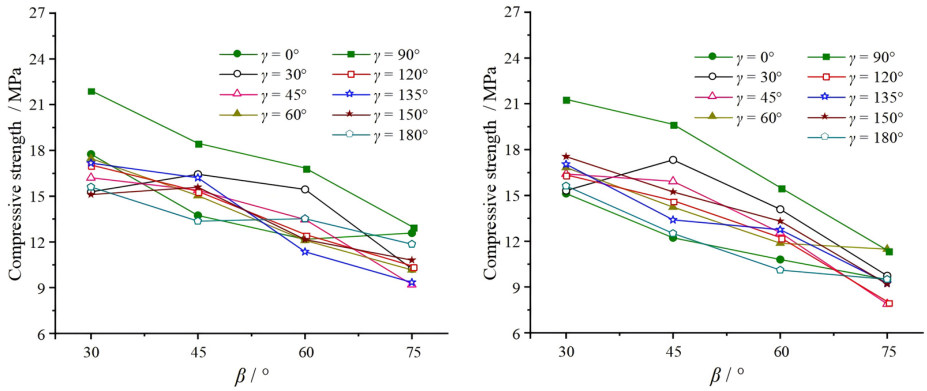

(c) (d)

Fig. 4. Influence of various β on the uniaxial compressive strength of the specimens for selected n and γ: (a) $n = 1$; (b) $n = 2$; (c) $n = 3$; (d) $n = 4$

Figure 4 illustrates the variation in compressive strength of the rock mass with respect to the angle β, while the orientation angle γ and the parameter n remain constant. As β increases from 30° to 75°, the wavelength of the regular asperities is maintained at 20 mm. Under these conditions, the effective inclination and the undulation amplitude of the structural plane increase correspondingly, resulting in a progressive reduction in compressive strength.

3.3. Influence of *n* on the compressive strength of the specimens

Figure 5 shows the influence of n on the uniaxial compressive strength of the rock mass specimens with dentate discontinuity when γ and β remained unchanged.

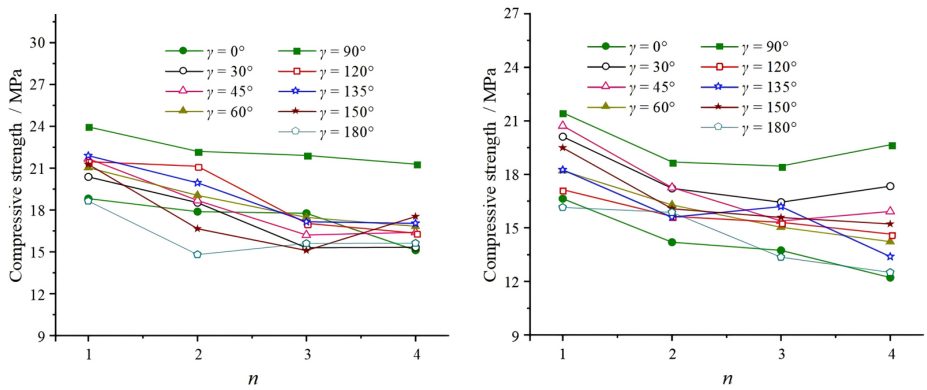

(a) (b)

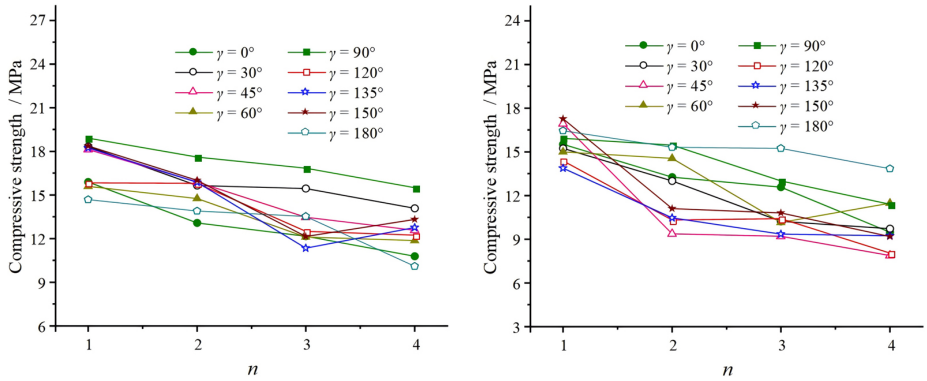

Fig. 5. Influence of n on the uniaxial compressive strength of the specimens for selected γ and β: (a) $\beta = 30°$; (b) $\beta = 45°$; (c) $\beta = 60°$; (d) $\beta = 75°$

As shown in Figure 5, the uniaxial compressive strength of the specimens with dentate discontinuity gradually decreased with an increase in n from 1 to 4 when γ and β of the specimens remained unchanged.

4. Uniaxial compression experiment and numerical simulation of the rock mass with joint fractures

4.1. Numerical simulation

In the PFC program, the particles are round, rigid bodies of particular masses. In the simulation process, the particles are not limited by deformation variables and can effectively reflect the mechanism, process, and results of material damage. Therefore, this method has been widely used by researchers to compensate for mechanical problems associated with discontinuous phenomena such as rock bursting.

A uniaxial compression test simulation was conducted on a rock sample with serrated surfaces using PFC2D. A 100 mm × 100 mm was established, consisting of 6468 circular particles of varying sizes. The particle radii were uniformly distributed between a specified maximum and minimum value. Regarding boundary conditions, the bottom plate of the model was fixed, while the top plate was moved downward at a constant rate, replicating the standard uniaxial compression test procedure. Inter-particle contact was modeled using the Parallel Bond Model. Prior to formal simulation, the micro-parameters of the model specimen were systematically calibrated based on the macro-mechanical parameters of the intact rock mass to ensure numerical responses aligned with physical test results, as shown in Table 3.

Table 3. Partial parameters of PFC material

Minimum particle radius (mm)	Maximum particle radius (mm)	Density ($g \cdot m^{-3}$)	Effective modulus (GPa)	Stiffness ratio	Coefficient of friction
1.0	1.66	1.96	1.4	1.0	0.5

Figure 6 shows the experimental and numerical results of failure characteristics of the rock mass specimens with dentate discontinuity when $n = 1$, $\gamma = 60°$, and $\beta = 75°$. The results were essentially consistent in terms of crack initiation, crack propagation, and crack coalescence. Therefore, numerical simulation is essential for uniaxial compression specimens with dentate discontinuity.

(a) (b)

Fig. 6. Comparison of experiment results and numerical simulation of the failure characteristics of the rock mass specimens with dentate discontinuity

4.2. Influence of γ on the compressive strength of the specimen numerical simulation

Figure 7 shows the influence of various γ on the numerical simulation results of the uniaxial compressive strength of the rock mass specimens with dentate discontinuity when n and β remained unchanged.

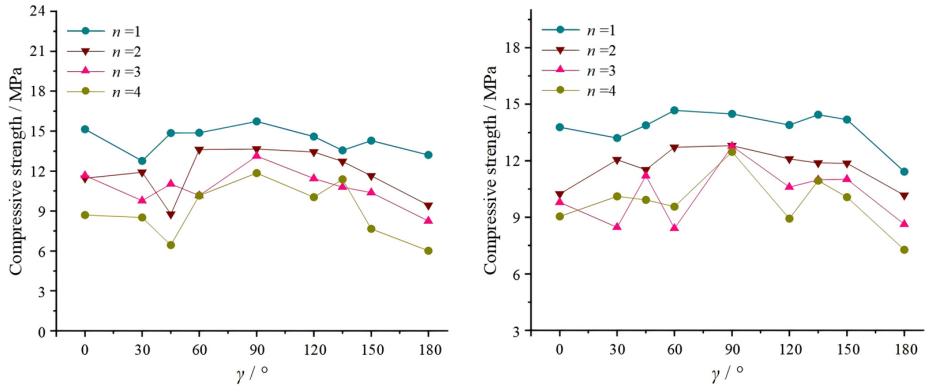

(a) (b)

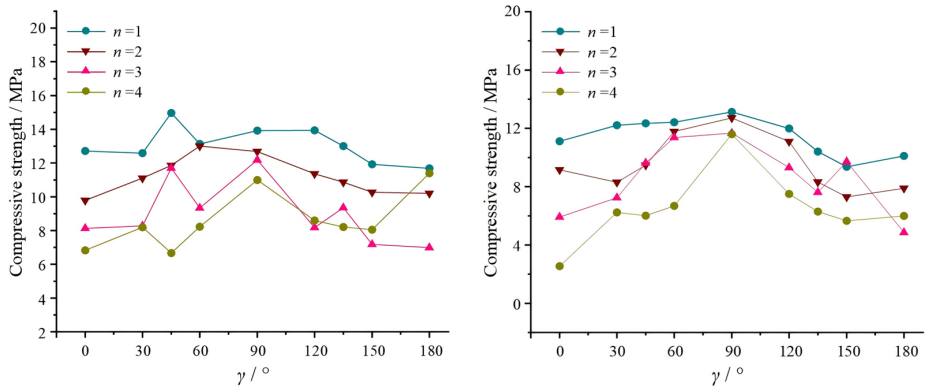

(c) (d)

Fig. 7. Influence of various γ on the numerical simulation results of the uniaxial compressive strength of the rock mass specimens for each selected n and β: (a) $\beta = 30°$; (b) $\beta = 45°$; (c) $\beta = 60°$; (d) $\beta = 75°$

As shown in the Figure 7, when n and β remained unchanged, the compressive strength of the irregular dentate discontinuity rock mass specimens was maximized at $\gamma = 90°$. The uniaxial compressive strength of the rock mass with dentate discontinuity increased as γ increased from 0° to 90° and decreased as γ increased from 90° to 180°. These results are consistent with the experimental results.

4.3. Effect of β on the numerical simulation results of the compressive strength of the specimens

Figure 8 shows the influence of various β on the numerical simulation results of the uniaxial compressive strength of the rock mass specimens with dentate discontinuity when n and γ remained unchanged.

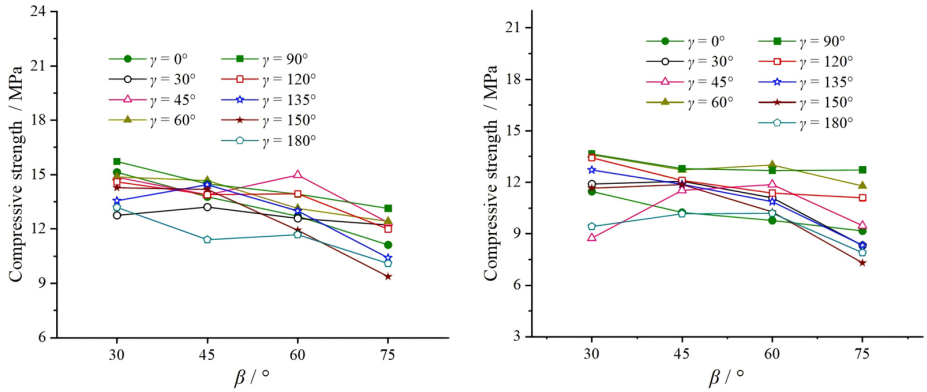

(a) (b)

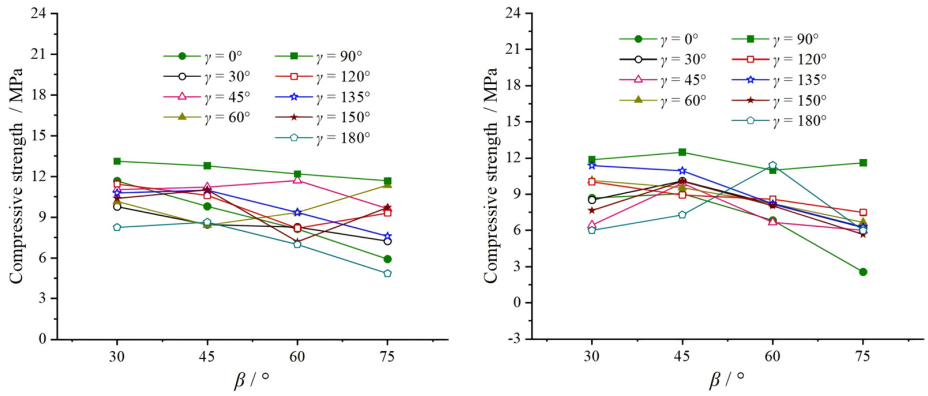

(c) (d)

Fig. 8. Influence of various β on the numerical simulation results of the uniaxial compressive strength of the rock mass specimens for selected n and γ: (a) $n = 1$; (b) $n = 2$; (c) $n = 3$; (d) $n = 4$

As shown in the Figure 8, when γ and n remained unchanged, the simulated strength of the rock mass specimens with dentate discontinuity decreased gradually as β increased from 30° to 75°, which is consistent with the experimental results of those with dentate discontinuity.

4.4. Effect of n on the numerical simulation results of the compressive strength of the specimens

Figure 9 shows the influence of various n on the numerical simulation results of the uniaxial compressive strength of the rock mass specimens with dentate discontinuity when γ and β remained the same.

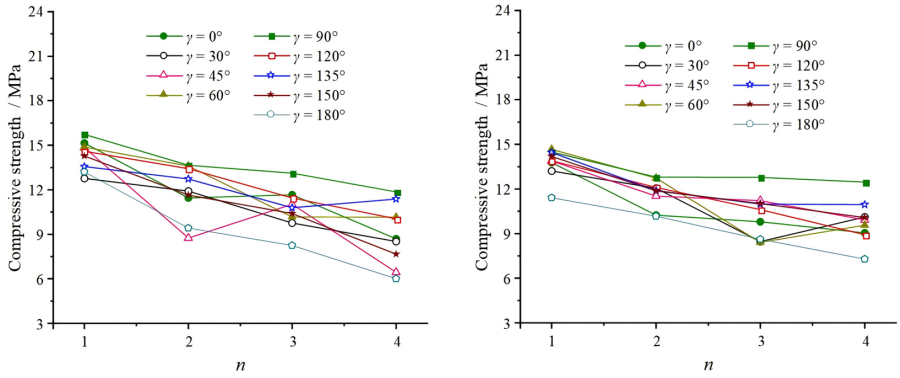

(a) (b)

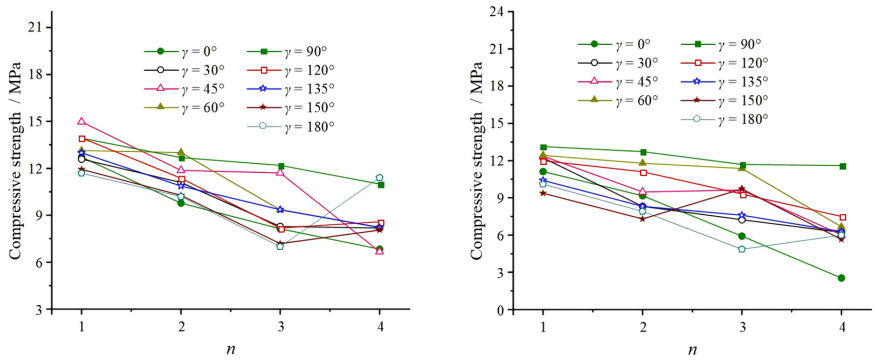

(c) (d)

Fig. 9. Influence of various n on the numerical simulation results of the uniaxial compressive strength of the rock mass specimens for selected γ and β: (a) $\beta = 30°$; (b) $\beta = 45°$; (c) $\beta = 60°$; (d) $\beta = 75°$

As shown in the Figure 9, when γ and β remained unchanged, the simulated strength of the rock mass specimens with dentate discontinuity decreased gradually as n increased from 1 to 4, which is consistent with the experimental results.

4.5. Comparative analysis of failure characteristics of test and numerical simulation

In both the experiments and the numerical simulation, almost all new cracks were initiated at the tip of the prefabricated crack, with a few initiated at the middle of or far from the prefabricated crack. The types of crack propagation include tensile, shear, and tension–shear composite cracking.

Figure 10 shows the influence of various γ on the failure characteristics of the specimens in the experiments and numerical simulations when $n = 2$ and $\beta = 75°$.

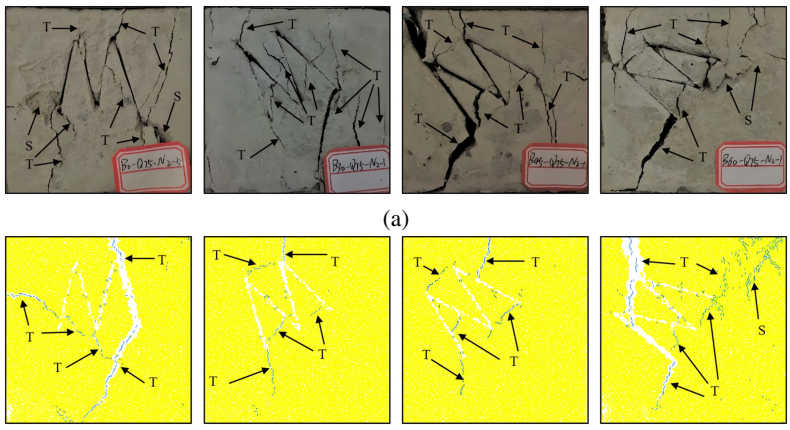

(a)

(b)

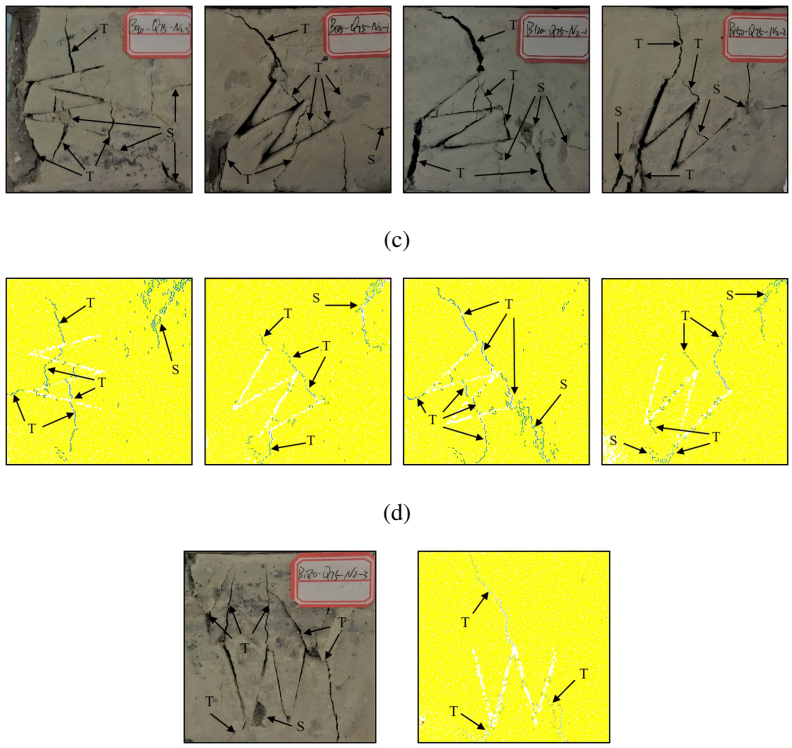

(c)

(d)

(e) (f)

Fig. 10. Influence of various γ on the failure characteristics of the rock mass specimens in the experiments and numerical simulations when $n = 2$ and $\beta = 75°$. In the panels, T and S represent tensile and shear cracking: (a) $\gamma = 0°$, $\gamma = 30°$, $\gamma = 45°$, $\gamma = 60°$; (b) $\gamma = 0°$, $\gamma = 30°$, $\gamma = 45°$, $\gamma = 60°$; (c) $\gamma = 90°$, $\gamma = 120°$, $\gamma = 135°$, $\gamma = 150°$; (d) $\gamma = 90°$, $\gamma = 120°$, $\gamma = 135°$, $\gamma = 150°$; (e) $\gamma = 180°$; (f) $\gamma = 180°$

Fig 10(a), (c) and (e) show failure characteristics of the experiment specimen, and (b), (d) and (f) show those observed in numerical simulation. When γ was 0°, 30°, 150°, and 180°, most of the new cracks originated at the tip of the prefabricated crack and propagated at an acute angle from the direction of the hypotenuse of the prefabricated crack. When γ was 90°, most of the new cracks originated at the middle of the prefabricated crack and propagated at a right angle from the direction of the hypotenuse of the prefabricated crack. When γ was 45°, 60°, 120°, and 135°, most of the new cracks began at the tip of the prefabricated crack and propagated at a right angle from the direction of the hypotenuse of the prefabricated crack. The failure of the rock mass specimens was mainly tensile crack type, and the coalescence direction of cracks eventually tended to follow the axial direction. When γ was 30°, 45°, 60°, 90°, 120°, 135°, and 150°, several new cracks were initiated at a distance from the prefabricated crack.

Figure 11 shows the influence of various β on the failure characteristics of the specimens in the experiments and numerical simulations when $n = 4$ and $\gamma = 180°$.

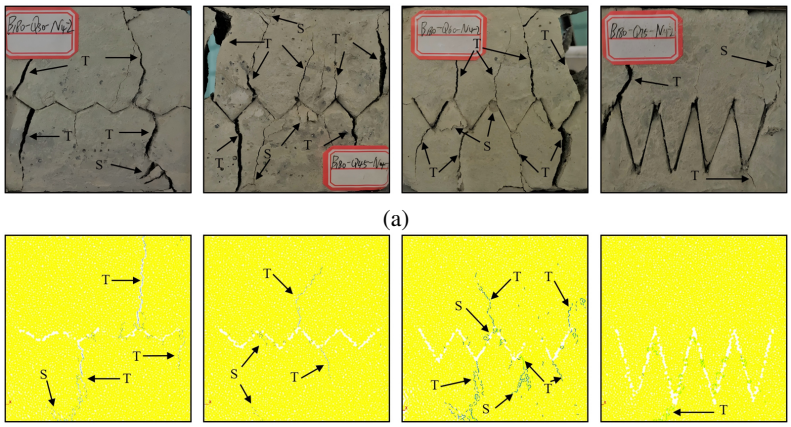

(a)

(b)

Fig. 11. Influence of various β on the failure characteristic of the rock mass specimens in the experiments and numerical simulations when $n = 4$ and $\gamma = 180°$: (a) $\beta = 30°$, $\beta = 45°$, $\beta = 60°$, $\beta = 75°$; (b) $\beta = 30°$, $\beta = 45°$, $\beta = 60°$, $\beta = 75°$

Figure 11(a) show the failure characteristics in the experiment specimens, and (b) show those of the numerical simulation. When β was 30°, 45°, and 60°, the new cracks initiated mainly at the tip of the prefabricated crack. The failure of rock mass specimens was dominated by tensile cracks; the new cracks were distributed evenly and symmetrically. A few shear cracks formed at the prefabricated crack tip owing to the stress concentration occurring at both ends of the prefabricated crack. When $\beta = 75°$, the failure form of the specimens was relatively simple, with only a small number of cracks initiating at the tip of the prefabricated crack.

Figure 12 shows the influence of various n on the failure characteristics of the specimens in the experiments and numerical simulations when $\beta = 75°$ and $\gamma = 60°$.

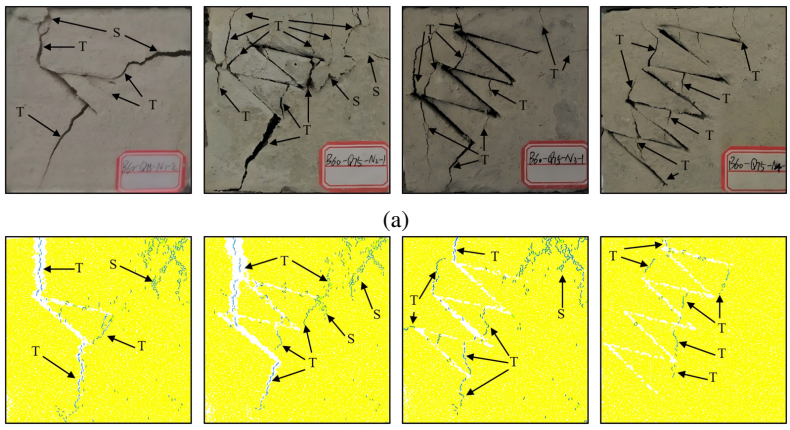

(a)

(b)

Fig. 12. Influence of various n on the failure characteristic of the rock mass specimens in the experiments and numerical simulations when $\beta = 75°$ and $\gamma = 60°$: (a) $n = 1$, $n = 2$, $n = 3$, $n = 4$; (b) $n = 1$, $n = 2$, $n = 3$, $n = 4$

Figure 12(a) show the failure characteristics of the experiment specimens, and (b) show those of the numerical simulation. When n was 1, 2, and 3, the tensile cracks were initiated mainly at the tip of the prefabricated crack, and the shear cracks began at the edges of the specimens far from the prefabricated crack. The new cracks propagated at a right angle from the direction of the hypotenuse of the prefabricated crack. When $n = 4$, the coalescence of the new cracks was not obvious.

5. Conclusions

Through uniaxial compression tests and particle flow numerical simulations on cement mortar specimens, this study investigates the influence of the rock mass dip angle γ, undulation angle β, and the number of undulating structures n on the compressive strength, along with the initiation and propagation patterns of cracks.

1. When the number of the undulating structures and the undulating angles remain unchanged, the uniaxial compressive strength of the rock mass specimens with regular dentate discontinuities peaks at a γ of 90°. As γ goes from 0° to 180°, their uniaxial compressive strength first increases and then decreases, and the uniaxial compressive strength is maximum at 90°.
2. When γ and β remain unchanged, the compressive strength of the rock mass specimens with dentate discontinuities all decrease with an increase in n.
3. When n and γ of undulating structures are known, the compressive strength of the rock mass specimens containing dentate discontinuity decreases with an increase in β.
4. Almost all of the new cracks in the rock mass specimens with regular dentate discontinuities are initiated at the tip of the prefabricated crack, with a few beginning at the middle of or far from the prefabricated crack. The failure characteristics of the rock mass are associated mainly with tensile cracks accompanied by a few shear cracks.
5. When the undulation angle and the number of undulating structures remain unchanged and the dip angle is 45°–135°, the crack in the rock mass with dentate discontinuity propagates first at a right angle from the direction of the hypotenuse of the preformed crack and finally propagates axially. When the dip angle and the number of undulating structures remain unchanged, the crack propagation of rock mass with $\beta \leq 60°$ is abundant. When γ and β remain unchanged and $n < 4$, the crack propagation is abundant and shear cracks are initiated at the edge of the specimens far from the prefabricated crack.

Acknowledgements

This work was supported by t the Open Research Fund of State Key Laboratory of Geohazard Prevention and Geoenvironment Protection (Grant no. SKLGP2021K020) and the Open Research Fund of Engineering Research Center of Underground Mine Construction, Ministry of Education (Grant No. JYBGCZX2020101).

References

[1] W.F. Brace and E.G. Bombolakis, "A note on brittle crack growth in compression", *Journal of Geophysical Research*, vol. 68, no. 12, pp. 3709–3713, 1963, doi: 10.1029/jz068i012p03709.

[2] H. Horii and S. Nemat-Nasser, "Compression-induced microcrack growth in brittle solids: axial splitting and shear failure", *Journal of Geophysical Research*, vol. 90, no. B4, pp. 3105–3125, 1985, doi: 10.1029/jb090ib04p03105.

[3] H. Horii and S. Nemat-Nasser, "Brittle failure in compression: splitting, faulting and brittle-ductile transition", *Philosophical Transactions of the Royal Society of London*, vol. 319, no. 1549, pp. 337–374, 1986, doi: 10.1098/rsta.1986.0101.

[4] M.F. Ashby and S.D. Hallam, "The failure of brittle solids containing small cracks under compressive stress states", *Acta Metallurgica*, vol. 34, no. 3, pp. 497–510, 1986, doi: 10.1016/0001-6160(86)90086-6.

[5] A. Bobet and H.H. Einstein, "Fracture coalescence in rock-type materials under uniaxial and biaxial compression", *International Journal of Rock Mechanics and Mining Sciences*, vol. 35, no. 7, pp. 863–888, 1998, doi: 10.1016/S0148-9062(98)00005-9.

[6] R.H.C. Wong and K.T. Chau, "Crack coalescence in a rock-like material containing two cracks", *International Journal of Rock Mechanics and Mining Sciences*, vol. 35, no. 2, pp. 147–164, 1998, doi: 10.1016/S0148-9062(97)00303-3.

[7] H. Lee and S. Jeon, "An experimental and numerical study of fracture coalescence in pre-cracked specimens under uniaxial compression", *International Journal of Solids and Structures*, vol. 48, no. 6, pp. 979–999, 2011, doi: 10.1016/j.ijsolstr.2010.12.001.

[8] H. Zhang, C. Yuan, S. Chen, G. Yang, and H. Xia, "Experimental study of fracture geometry characteristics on rock mass strength and crack propagation evolution law", *European Journal of Environmental and Civil Engineering*, vol. 26, no. 16, pp. 7972–8001, 2022, doi: 10.1080/19648189.2021.2015448.

[9] J. Qi, L. Zhou, H. Zhang, J. Chen, L. Ma, and T. Shi, "Research on crack evolution law and mechanical analysis of three cracked rock masses subjected to compression load", *Theoretical and Applied Fracture Mechanics*, vol. 127, art. no. 104035, 2023, doi: 10.1016/j.tafmec.2023.104035.

[10] J.K. Kodikara and I.W. Johnston, "Shear behaviour of irregular triangular rock-concrete joints", *International Journal of Rock Mechanics and Mining Sciences & Geomechanics Abstracts*, vol. 31, no. 4, pp. 313–322, 1994, doi: 10.1016/0148-9062(94)90900-8.

[11] C.M. Haberfield and I.W. Johnston, "A mechanistically-based model for rough rock joints", *International Journal of Rock Mechanics and Mining Sciences & Geomechanics Abstracts*, vol. 31, no. 4, pp. 279–292, 1994, doi: 10.1016/0148-9062(94)90898-2.

[12] F. Homand, T. Belem, and M. Souley, "Friction and degradation of rock joint surfaces under shear loads", *International Journal for Numerical and Analytical Methods in Geomechanics*, vol. 25, no. 10, pp. 973–999, 2001, doi: 10.1002/nag.163.

[13] T.H. Kwon, E.S. Hong, and G.C. Cho, "Shear behavior of rectangular-shaped asperities in rock joints", *KSCE Journal of Civil Engineering*, vol. 14, no. 3, pp. 323–332, 2010, doi: 10.1007/s12205-010-0323-1.

[14] pp. M. Bahaaddini, G. Sharrock, and B.K. Hebblewhite, "Numerical direct shear tests to model the shear behaviour of rock joints", *Computers and Geotechnics*, vol. 51, pp. 101–115, 2013, doi: 10.1016/j.compgeo.2013.02.003.

[15] M. Bahaaddini, P.C. Hagan, R. Mitra, and B.K. Hebblewhite, "Scale effect on the shear behaviour of rock Joints based on a numerical study", *Engineering Geology*, vol. 181, pp. 212–223, 2014, doi: 10.1016/j.enggeo.2014.07.018.

[16] Q. Yin, X. Nie, J. Wu, Q. Wang, K. Bian, and H. Jing, "Experimental study on unloading induced shear performances of 3D saw-tooth rock fractures", *International Journal of Mining Science and Technology*, vol. 33, no. 4, pp. 463–479, 2023, doi: 10.1016/j.ijmst.2023.02.002.

[17] X. Li, et al., "Study on shear mechanical properties and fracture evolution mechanism of irregular serrated rock discontinuities", *Applied Sciences*, vol. 13, no. 4, art. no. 2444, 2023, doi: 10.3390/app13042444.

Received: 2023-08-09, Revised: 2025-09-15